PEROVSKITES

Three-dimensional direct lithography of stable perovskite nanocrystals in glass

Ke Sun[1]†, Dezhi Tan[2]*†, Xinyuan Fang[3,4]†, Xintao Xia[1], Dajun Lin[3,4], Juan Song[5], Yonghong Lin[6], Zhaojun Liu[6], Min Gu[3,4], Yuanzheng Yue[7], Jianrong Qiu[1,8]*

Material composition engineering and device fabrication of perovskite nanocrystals (PNCs) in solution can introduce organic contamination and entail several synthetic, processing, and stabilization steps. We report three-dimensional (3D) direct lithography of PNCs with tunable composition and bandgap in glass. The halide ion distribution was controlled at the nanoscale with ultrafast laser–induced liquid nanophase separation. The PNCs exhibit notable stability against ultraviolet irradiation, organic solution, and high temperatures (up to 250°C). Printed 3D structures in glass were used for optical storage, micro–light emitting diodes, and holographic displays. The proposed mechanisms of both PNC formation and composition tunability were verified.

Compositional tuning of the optical properties of perovskites (*1*, *2*) is usually performed in solution to create materials for high-performance devices with long-term stability (*3*–*5*), such as mixed chloride-bromide and bromide-iodide perovskites for spectrally stable and high-efficiency blue and red light-emitting diodes (LEDs), respectively (*5*, *6*). Despite recent advances in optoelectrical performance, low structural stability has been an obstacle for practical perovskite devices (*6*), and numerous strategies such as surface passivation or device encapsulation have been developed (*7*). In these approaches, stabilization requires additional processing steps at the thin film or device level and is not integral to tuning the nanocrystal (NC) properties.

The postsynthetic incorporation of NCs into glass has led to advanced photonic functionalities (*8*, *9*). However, the three-dimensional (3D) tailoring of the chemical composition and the bandgap of NCs inside glass, and, in turn, the tuning of the functionalities of NC-based photonic devices, is challenging. Recently, an ultrafast laser has been used to fabricate 3D functional structures in transparent solids (*10*–*13*), but the internal composition tunability of functional structures is rather limited.

We report a different strategy for engineering the local chemistry of NCs. Specifically, ultrafast-laser pulses inject energy within an ultrashort amount of time, which leads to strong thermal accumulation and thereby increases the local pressure and temperature above the liquidus of the studied glass system to induce localized liquid nanophase separation (*14*–*16*), so that 3D direct lithography of composition-tunable perovskite NCs (PNCs) inside glass is realized (Fig. 1A). The mechanism of the composition tuning of PNCs through liquid nanophase separation was clarified. In addition, our approach enabled the PNCs to be well protected against high-power ultraviolet (UV) light irradiation, organic solution, or temperatures up to 250°C.

We used oxide glasses containing cesium, lead, and halide elements as our medium for direct lithography of PNCs. As a typical oxide glass, borophosphate glass with the molar composition of $40B_2O_3$-$15P_2O_5$-$10Al_2O_3$-$10ZnO$-$5Na_2O$-$5K_2O$-$7Cs_2O$-$3PbX_2$-$5NaX$ (where X is Cl, Br, or I) was prepared using a melt-quenching method. The high mobility of cesium, lead, and halide ions promotes perovskite nanophase separation from the glass matrix and the subsequent formation of compositionally tunable PNCs (*4*, *5*, *16*). We achieved the

[1]State Key Laboratory of Modern Optical Instrumentation, College of Optical Science and Engineering, Zhejiang University, Hangzhou, China. [2]Zhejiang Lab, Hangzhou, China. [3]Institute of Photonic Chips, University of Shanghai for Science and Technology, Shanghai, China. [4]Centre for Artificial-Intelligence Nanophotonics, School of Optical-Electrical and Computer Engineering, University of Shanghai for Science and Technology, Shanghai, China. [5]College of Materials Science and Engineering, Jiangsu University, Zhenjiang, China. [6]Department of Electrical and Electronic Engineering, Southern University of Science and Technology, Shenzhen 518055, China. [7]Department of Chemistry and Bioscience, Aalborg University, 9220 Aalborg, Denmark. [8]CAS Center for Excellence in Ultra-intense Laser Science, Chinese Academy of Sciences, Shanghai 201800, China.
***Corresponding author. Email: wctdz@zju.edu.cn (D.T.); qjr@zju.edu.cn (J.Q.)**
†These authors contributed equally to this work.

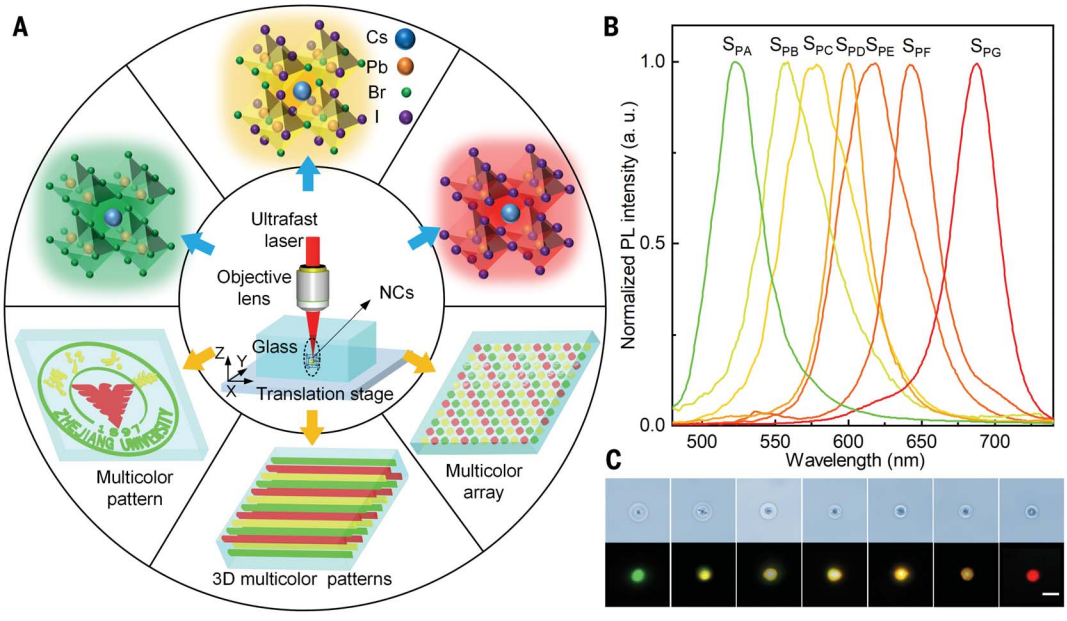

Fig. 1. Direct lithography of composition-tunable PNCs in glass. (**A**) Schematic illustration of direct lithography of colored PNCs and patterns. (**B**) PL spectra of $CsPb(Br_{1-x}I_x)_3$ PNCs written in one piece of glass. S_{PA} to S_{PG} represent the samples of $CsPb(Br_{1-x}I_x)_3$ written with different laser parameters that are shown in table S1. a.u., arbitrary units. (**C**) Optical images (top) and PL mappings (bottom) of $CsPb(Br_{1-x}I_x)_3$ NCs. The scale bar is 10 μm, and the excitation wavelength is 405 nm.

desired ultrafast-laser direct lithography process by optimizing the pulse duration, repetition rate, and pulse energy (table S1). The photoluminescence (PL) of the as-prepared PNCs was tuned across the wavelength range from 520 to 690 nm (Fig. 1B). The light emissions at 520 and 690 nm were attributed to the exciton recombination in $CsPbBr_3$ and $CsPbI_3$ NCs, respectively, and the emissions between these two wavelengths originated from the mixed halide $CsPb(Br_{1-x}I_x)_3$ NCs (*1*, *2*), where x was determined using Vegard's law (fig. S1). The presence of PNCs was confirmed by both the transmission electron microscopy images (fig. S2) and Raman spectra (fig. S3), and the mean size of the PNCs was determined to be between 1 and 4 nm.

We realized control over the dynamical process of liquid nanophase separation by adjusting the ultrafast-laser irradiation time (t_i) (Fig. 2A). Here, the halide ion migration rate depends on the complexation between Pb^{2+} and halide ions and the radius and weight of ions (*17*, *18*). In comparison with I^-, a greater complexation between Pb^{2+} and Br^-, lighter ionic weight, and smaller radius allowed for faster diffusion of Br^- and easier formation of Br-rich liquid perovskite through nanophase separation. Continuous irradiation allowed more I^- ions to diffuse into the liquid perovskite region from the liquid-glass domains and enabled tuning of the emission of the final PNCs (Fig. 2B and supplementary text S2) from green to red by extending t_i.

To validate our approach, $CsPb(Cl_{1-x}Br_x)_3$ NCs were generated in glass, and the emission was tuned across a wide wavelength range from 450 to 514 nm (fig. S4) by controlling the laser parameters (table S3). Furthermore, we succeeded in engineering the composition and bandgap of PNCs in the Cl^--Br^--I^- codoped glass. Thus, the full-color printing of PNCs (fig. S5) with PL tuned in a range from 480 to 700 nm was achieved (Fig. 2C) and reflected the transformation of $CsPb(Cl_{1-x}Br_x)_3$ into $CsPbI_3$, thus confirming the PNC composition engineering. The PL of PNCs written in both Cl^--Br^- (fig. S6) doped glasses and Cl^--Br^--I^- (fig. S7) doped glasses (fig. S7) were continuously modulated by changing t_i, and, specifically, the main PL peak shifted to longer wavelengths with an increase in t_i. Regulation of the halide ion distribution in PNCs in glass was not possible through a conventional homogeneous heat treatment (fig. S8).

Phase separation occurs in glass-forming systems if a chemical potential gradient exists. Based on our experimental findings, here we propose the mechanism of PNC formation through nanophase separation by taking Br^--I^- doped glass as an example (Fig. 2A). First, formation of immiscible phases resulted in liquid phase separation at the nanoscale level. Thus, separation of the Br-rich halide phase from the glass matrix phase occurred at temperatures above the liquidus temperature of the glass composition (*19*). Second, continuous ultrafast-laser irradiation not only increased the size of the liquid perovskite domains (fig. S9) but also induced the site exchange of I to Br owing to the chemical potential gradient (Fig. 2A) (*20*). As the laser irradiation proceeded, I^-

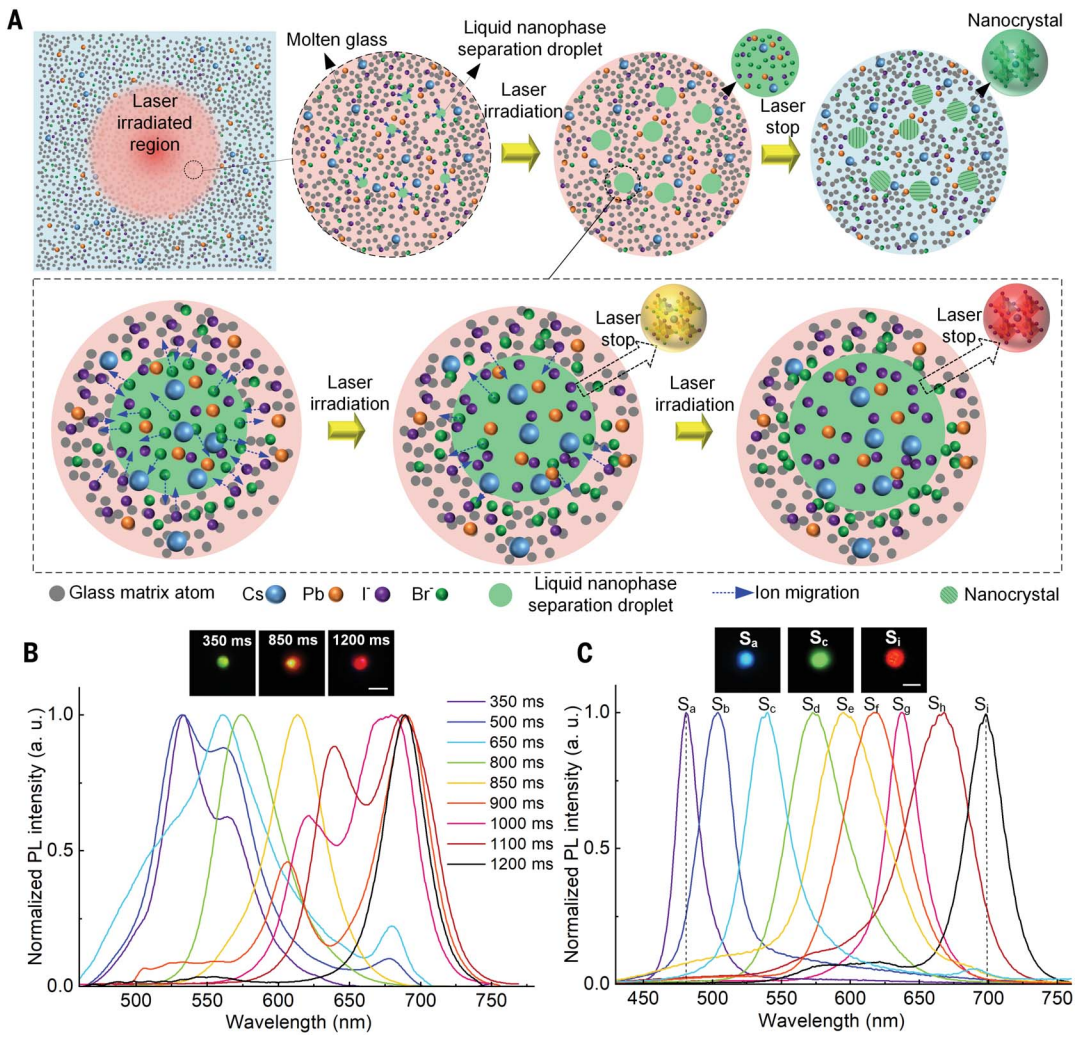

Fig. 2. Dynamical control over the halide ion migration and full-color printing of PNCs. (**A**) Schematic of ultrafast laser–induced liquid nanophase separation and formation of $CsPb(Br_{1-x}I_x)_3$ NCs in the Br^--I^- doped glass. (**B**) PL mappings and PL spectra of $CsPb(Br_{1-x}I_x)_3$ NCs as a function of t_i. The ultrafast-laser repetition rate is 125 kHz, the pulse duration is 885 fs, and the pulse energy is 400 nJ. (**C**) PL mappings and PL spectra of PNCs written in the Cl^--Br^--I^- codoped glass. S_a to S_i represent the PNC samples written in the Cl^--Br^--I^- codoped glass with different laser parameters that are shown in table S2.

ions gradually diffused from the surrounding liquid to the relatively ordered liquid perovskite domains, finally leading to the formation of I^--containing liquid perovskite nanodomains. The nanophase separation lowered the energy barrier for formation of the domains with a preordered perovskite-like structure (*21*). Third, the preordered liquid perovskite domains became more ordered and created the crystallization nuclei that subsequently grew into PNCs through diffusion and reaction in a confined manner during the cooling process (*22*).

During ultrafast-laser direct lithography, the temperature of the laser-impacted domains increased rapidly with the number of pulses and remained stable at the maximum after several tens of pulses (typically less than 100 pulses that correspond to a t_i of 1 ms for a 100-kHz ultrafast laser). A quenching process occurred after shutting off the ultrafast-laser irradiation (*23*). The ultrafast laser–induced temperature (>1000°C; fig. S10) in the modified area is above the liquidus of the glass composition (fig. S11). Thus, the dependence of the emission wavelength of PNCs on t_i verified the occurrence of liquid nanophase separation. The mean size of $CsPb(Br_{1-x}I_x)_3$ NCs increased from 1.9 to 3.6 nm with an increase in t_i from 350 to 1200 ms (fig. S9), which provided a clear signature of the continuous localized liquid nanophase separation.

The distinct evolution of PNCs (Fig. 2B and figs. S12 to S14) with adjusted ultrafast-laser parameters could be related to the differences in temperature (fig. S10), pressure, and irradiance of the ultrafast laser. For example, the phase diagram depended on the pressure, and the liquid phase separation could be facilitated by increasing the pressure up to a gigapascal level (*14*–*16*, *24*, *25*). These features account, in part, for why ultrafast-laser heating could drive liquid nanophase separation, whereas the normal heat treatment could not.

The instability of PNCs can occur through chemical- and thermal-induced decomposition as well as light-induced phase segregation (*7*, *17*, *26*). We investigated the stability of PNCs against UV irradiation, heat treatment, or solvent (ethanol) exposure. All of the PNCs that emitted green, yellow, orange, and red PL were stable, and no change in PL intensity was observed after UV irradiation for 12 hours (Fig. 3A). Furthermore, there was also no PL peak shift when $CsPb(Br_{1-x}I_x)_3$ NCs were irradiated by UV light with the power density (I_{UV}) of 2 W/cm^2 (Fig. 3B) and even 32 W/cm^2 (figs. S15 and S16), implying an absence of phase segregation. As a reference, UV light with an I_{UV} of 0.1 W/cm^2 can induce substantial phase segregation in mixed-halide perovskites (*4*, *5*, *17*).

The PNCs remained stable when dispersed in ethanol without a change in the PL quantum yield after 6 months (Fig. 3C). The PL intensity and position of PNCs also remained as the initial characteristics after they were heat-treated at 85°C for 960 hours (Fig. 3D and fig. S17) and even after heat treatment at 250°C for 2 hours under atmospheric conditions (fig. S18). The high stability of PNCs originates from the effective protection of the glass matrix that prevents the as-written PNCs from being attacked by molecules in the surrounding environment at various temperatures (supplementary text S5) (*7*). Furthermore, the factors, such as nanoconfinement, ultrafast laser–induced residual strain, high surface-to-volume ratio, high cohesive energy, and limited carrier diffusion length given the small size of PNCs could lead to strong suppression of the ion diffusion and UV light–induced phase segregation (*10*, *17*, *27*, *28*).

Writing composition-tunable PNCs allows for applications in multidimensional information encoding and anticounterfeiting (Fig. 1A and fig. S19). For example, green, yellow, and red logos of Zhejiang University were directly written in glass (Fig. 4, A to C). Figure 4, D and E, shows the colorful patterns that are produced with $CsPb(Br_{1-x}I_x)_3$ NCs and $CsPb(Cl_{1-x}Br_x)_3$ NCs, respectively, in the corresponding glasses. We also demonstrated full-color printing of PNCs in the Cl^--Br^--I^- codoped glass (Fig. 4F) and 3D microhelix PNC patterns (Fig. 4G).

Micrometer-scale LEDs (μ-LEDs) for high-resolution display have been fabricated with wet chemistry–derived NCs (*29*, *30*). For standard NC-based devices, dots with different emission wavelengths were printed or transferred on substrates, and the NC preparation and device manufacturing were complicated (*29*). Thus, the cost of device fabrication is high, the stability of NCs can be low, and NC patterning is difficult. These drawbacks severely limit the wide applications of NC-based devices. In addition, although considerable efforts were made to exploit glasses as light-emitting materials and devices (*10*, *31*, *32*), it has not been

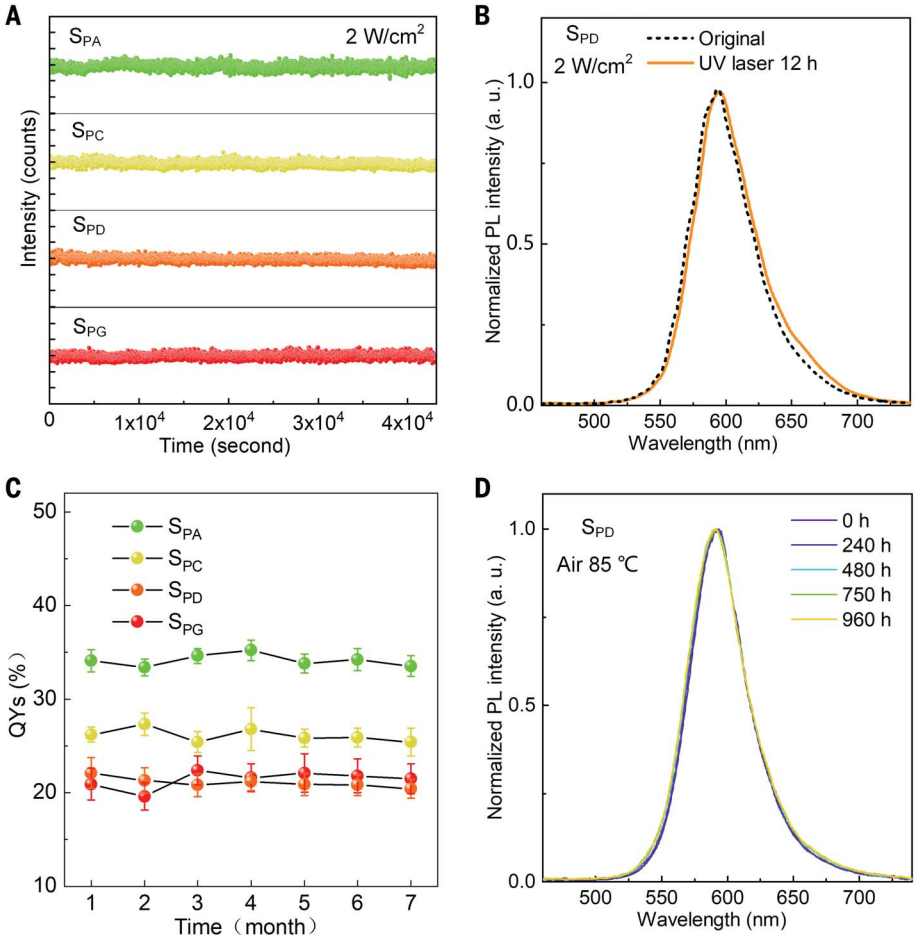

Fig. 3. Stability of $CsPb(Br_{1-x}I_x)_3$ NCs. (**A**) PL intensity of $CsPb(Br_{1-x}I_x)_3$ NCs illuminated for 12 hours by UV laser with an I_{UV} of 2 W/cm^2. (**B**) PL spectra of S_{PD} NCs before and after irradiation. (**C**) PL quantum yields (QYs) of $CsPb(Br_{1-x}I_x)_3$ NCs dispersed in ethanol after 6 months. Error bars represent standard deviation. (**D**) PL spectra of S_{PD} NCs after heat treatment at 85°C for 960 hours.

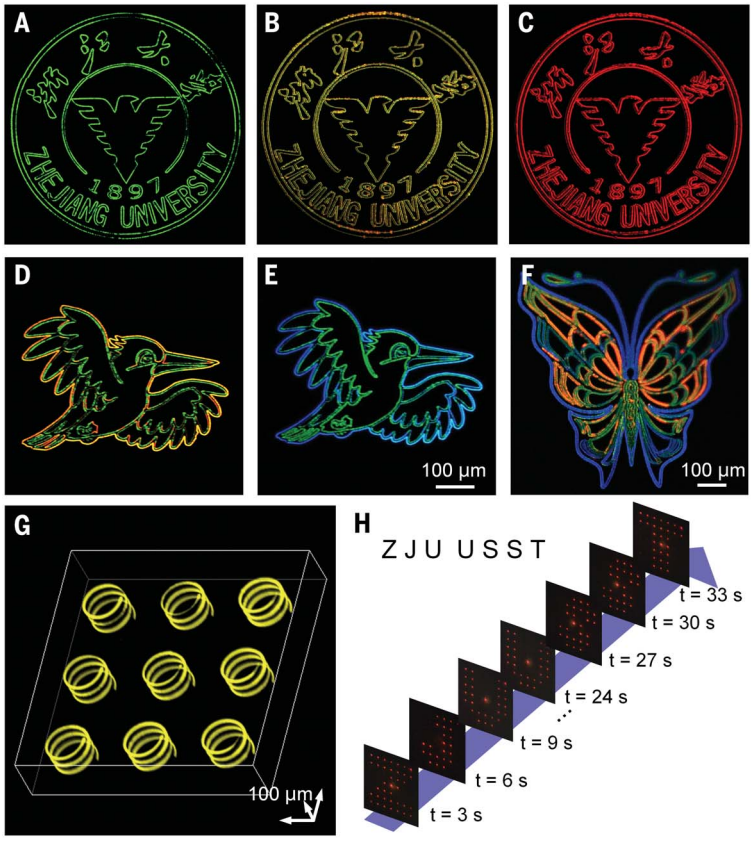

Fig. 4. Direct lithography of PNC patterns and devices. (**A** to **C**) Zhejiang University logos based on $CsPb(Br_{1-x}I_x)_3$ NCs with varied compositions in one piece of glass. (**D** to **F**) Typical PL images of the multicolor patterns produced with $CsPb(Br_{1-x}I_x)_3$ NCs in the Br^--I^- doped glass (D), $CsPb(Cl_{1-x}Br_x)_3$ NCs in the Cl^--Br^- doped glass (E), and $CsPb(Cl_{1-x-y}Br_xI_y)_3$ NCs in the Cl^--Br^--I^- codoped glass (F). The colorful patterns were produced by adjusting the parameters during writing. (**G**) 3D microhelix $CsPb(Br_{1-x}I_x)_3$ NC arrays. The patterns were excited by UV light. (**H**) Demonstration of a dynamic holographic display. The letters at the top left represent the images shown at different times (t = 3, 6, 9, 24, 27, and 33 s, respectively) in the demonstration of a dynamic holographic display. The excitation wavelength is 532 nm. Scale bars in (A) to (F) are 100 μm.

possible to endow a single glass chip with widely and continuously tunable colors or to print NC-based devices such as μ-LEDs and displays inside solids (*5*, *29*).

The PNC-based glass can be used as the key component of photonic devices, not just as a transparent protection layer or substrate (*33*). We demonstrated one-step 3D printing of colored PNC patterns with a dot size <10 μm (fig. S20) that can be used for building micrometer-sized devices. Combining commercially available UV or blue LED arrays, this technology could apply to the fabrication of μ-LEDs (fig. S21), high-resolution displays, and even white LEDs (figs. S22 and S23) (*2*, *29*, *34*). Moreover, the PNC arrays were used as a holographic display device. Through the switching of holograms, the dynamic holographic display based on such a PNC-based device was achieved (Fig. 4H, fig. S24, and movie S1). Three holographic images (letters "Z," "J," and "U") were further reconstructed simultaneously in multiple planes along the light propagation direction, indicating that the excitation of specific PNC patterns enabled realization of a 3D holographic display (fig. S25).

Because liquid nanophase separation only occurs at a local position inside glass, the 3D direct lithography represents a completely dry fabrication technique that advances the fabrication of structures and devices with high throughput and high scalability. It excludes contamination with organic components (reagents and solvents) during material synthesis and device processing. Furthermore, the high-temperature stability indicates that the PNC glass-based devices can be applied for long-term applications (*35*). The present study demonstrates that the composition and bandgap of PNCs could be tailored over the entire tunable range in one single solid chip.

REFERENCES AND NOTES

1. L. Protesescu *et al*., *Nano Lett.* **15**, 3692–3696 (2015).
2. X. Li *et al*., *Adv. Funct. Mater.* **26**, 2435–2445 (2016).
3. D. P. McMeekin *et al*., *Science* **351**, 151–155 (2016).
4. J. Xu *et al*., *Science* **367**, 1097–1104 (2020).
5. Y. Hassan *et al*., *Nature* **591**, 72–77 (2021).
6. X.-K. Liu *et al*., *Nat. Mater.* **20**, 10–21 (2021).
7. Y. Wei, Z. Cheng, J. Lin, *Chem. Soc. Rev.* **48**, 310–350 (2019).
8. A. Llordés, G. Garcia, J. Gazquez, D. J. Milliron, *Nature* **500**, 323–326 (2013).
9. A. L. Efros, L. E. Brus, *ACS Nano* **15**, 6192–6210 (2021).
10. X. Huang *et al*., *Nat. Photonics* **14**, 82–88 (2020).
11. W. Yang, P. G. Kazansky, Y. P. Svirko, *Nat. Photonics* **2**, 99–104 (2008).
12. D. Z. Tan, Z. Wang, B. Xu, J. Qiu, *Adv. Photonics* **3**, 024002 (2021).
13. D. Wei *et al*., *Nat. Photonics* **12**, 596–600 (2018).
14. Y. Katayama *et al*., *Science* **306**, 848–851 (2004).
15. S. Aasland, P. F. McMillan, *Nature* **369**, 633–636 (1994).
16. E. D. Zanotto, *Ceram. Int.* **46**, 24779–24791 (2020).
17. M. C. Brennan, A. Ruth, P. V. Kamat, M. Kuno, *Trends Chem.* **2**, 282–301 (2020).
18. S. J. Yoon, K. G. Stamplecoskie, P. V. Kamat, *J. Phys. Chem. Lett.* **7**, 1368–1373 (2016).
19. P. F. James, *J. Mater. Sci.* **10**, 1802–1825 (1975).
20. G. Nedelcu *et al*., *Nano Lett.* **15**, 5635–5640 (2015).
21. Y. Yue, *J. Non-Cryst. Solids* **345–346**, 523–527 (2004).
22. M. Allix, L. Cormier, in *Springer Handbook of Glass*, J. D. Musgraves, J. Hu, L. Calvez, Eds. (Springer, 2019), chap. 4.
23. D. Z. Tan, B. Zhang, J. R. Qiu, *Laser Photonics Rev.* **15**, 2000455 (2021).
24. L. Henry *et al*., *Nature* **584**, 382–386 (2020).
25. K. H. Kim *et al*., *Science* **370**, 978–982 (2020).
26. M. Liu *et al*., *Nat. Photonics* **15**, 379–385 (2021).
27. X. Kong *et al*., *Nanoscale* **10**, 8320–8328 (2018).
28. X. Wang *et al*., *Nat. Commun.* **10**, 695 (2019).
29. Z. Liu *et al*., *Light Sci. Appl.* **9**, 83 (2020).
30. Y. Wang, I. Fedin, H. Zhang, D. V. Talapin, *Science* **357**, 385–388 (2017).
31. X. Liu, J. Zhou, S. Zhou, Y. Yue, J. Qiu, *Prog. Mater. Sci.* **97**, 38–96 (2018).
32. T. Hu *et al*., *Light Sci. Appl.* **10**, 56 (2021).
33. J. H. Choi *et al*., *Nat. Photonics* **5**, 763–769 (2011).
34. M. Zhao *et al*., *Light Sci. Appl.* **8**, 38 (2019).
35. J. Zhang, M. Gecevičius, M. Beresna, P. G. Kazansky, *Phys. Rev. Lett.* **112**, 033901 (2014).

ACKNOWLEDGMENTS

We thank Y. Zhang (Qilu University of Technology) for performing differential scanning calorimetry measurements. **Funding:** This work was financially supported by the National Natural Science Foundation of China (grant nos. U20A20211, 51902286, 61775192, 61905215, 51772270, and 62005164) and the Shanghai Frontiers Science Center Program 2021-2025 (NO.20). **Author contributions:** K.S., D.T., and X.F. contributed equally to this work. D.T. conceived the idea. J.Q. organized, coordinated, and supervised the project. K.S. and X.X. performed the experiments and collected the data. X.F. and D.L. carried out the holographic display experiment. Y.L. and Z.L. carried out the LED device experiment. J.S. performed the theoretical calculations. D.T., Y.Y., and J.Q. interpreted the results and proposed the mechanism of the composition engineering of perovskite nanocrystals in glass with a laser. D.T. wrote the manuscript. M.G. supervised the holographic display experiment and reviewed the manuscript. D.T., Y.Y., and J.Q. discussed and revised the manuscript. **Competing interests:** The authors declare no competing interests. **Data and materials availability:** All data needed to evaluate the conclusions in the paper are available in the main text or the supplementary materials.

SUPPLEMENTARY MATERIALS

science.org/doi/10.1126/science.abj2691
Materials and Methods
Supplementary Text
Figs. S1 to S41
Tables S1 to S6
References (*36*–*58*)
Movie S1

2 May 2021; resubmitted 13 October 2021
Accepted 2 December 2021
10.1126/science.abj2691

Science

Three-dimensional direct lithography of stable perovskite nanocrystals in glass

Ke SunDezhi TanXinyuan FangXintao XiaDajun LinJuan SongYonghong LinZhaojun LiuMin GuYuanzheng YueJianrong Qiu

Science, 375 (6578), • DOI: 10.1126/science.abj2691

Perovskite nanocrystals under glass

Perovskite nanocrystals (PNCs) such as cesium lead triiodide (CsPbI) can display bright photoemission with narrow linewidths for display applications, but their long-term stability requires passivation and encapsulation steps after synthesis in solution. Sun *et al*. created three-dimensional arrays of PNCs in doped metal oxide glasses using ultrafast laser pulses that caused local melting and subsequent crystallization. They tuned the bandgap of PNCs and their photoluminescence between 480- and 700-nanometer wavelengths by transforming the composition from CsPb(Cl Br) to CsPbI. These encapsulated PNCs exhibited long-term stability after prolonged heating or organic solvent and ultraviolet light exposure. —PDS